Preprint of an article published in International Journal of Bifurcation and Chaos, 26 (01), 1650018 (2016)
https://doi.org/10.1142/S0218127416500188

Analog electronic implementation of a class of hybrid dissipative dynamical system

L.J. Ontañón-García[a,*], E. Campos-Cantón[b], R. Femat[b]

[a] Coordinación Académica Región Altiplano Oeste,
Universidad Autónoma de San Luis Potosí,
Kilometro 1 carretera a Santo Domingo, 78600,
Salinas de Hidalgo, San Luis Potosí, México

[b] División de Matemáticas Aplicadas,
Instituto Potosino de Investigación Científica y Tecnológica A.C.
Camino a la Presa San José 2055 col. Lomas 4a Sección, 78216,
San Luis Potosí, SLP, México

Abstract

An analog electronic implementation by means of operational amplifiers of a class of hybrid dissipative systems in $\mathbf{R}^3$ is presented. The switching systems have two unstable hyperbolic focus-saddle equilibria with the same stability index, a positive real eigenvalue and a pair of complex conjugated eigenvalues with negative real part. The analog circuit generates signals that oscillate in an attractor located between the two unstable equilibria, and may present saturation states at the moment of energizing it, *i.e.*, if the initial voltage on the capacitors doesn't belong to the basin of attraction the circuit will end on a saturation state.

Keywords: Electronic implementation, piecewise linear systems, hybrid systems, analog computation, chaos.

1. Introduction

Hybrid dynamical systems are characterized by the mutual existence of continuous and discrete dynamics. This type of systems describes ~~behaviors of~~ in-

*Corresponding author
Email addresses: luis.ontanon@uaslp.mx (L.J. Ontañón-García), eric.campos@ipicyt.edu.mx (E. Campos-Cantón), rfemat@ipicyt.edu.mx (R. Femat)

teresting and somehow common phenomena such as switched electrical circuits and systems involving both digital and analog components, physical systems affected by impact, sliding or friction forces and stimulus-driven biological systems [1, 2]. Considering the latter systems, the mathematical modelling by hybrid dynamics results as an important tool for understanding the nonlinear dynamics of several biological and medical systems due to the many discontinuities they may present. Examples of this can relate on threshold–triggered firing in neurons, on–off switching of gene expression and division in cells among others [3, 4, 5].

An interesting example of hybrid dynamical systems is represented by piecewise linear (PWL) systems, particularly the ones described by the *unstable dissipative systems* (UDS) theory [6, 7, 8, 9]. The outline of this theory lies on the characterization of linear system onto two types depending on their eigenvalues. Considering switching systems with states lying in $\mathbf{R}^3$, the stability index of type I refers to one negative real eigenvalue and one pair of complex conjugated eigenvalues with positive real part. Likewise, the stability index of type II refers to one positive real eigenvalue and one pair of complex conjugated eigenvalues with negative real part.

Scientists have taken advantage of these types of indexes in the design of chaotic dissipative attractors by the adjustment of the location of their equilibria and their combination. The idea of the method started from the fact that almost any attractor reported so far in the literature presents a combination of equilibria that can be characterized between these two types of stability indexes depending on their eigenvalues. To account for this, one may consider the well known Lorenz system and the Chua's circuit reported in [10, 11]. These systems have three unstable equilibria corresponding to the following: one with stability index II located in the center and two with stability index I to the left and right sides. As it is known, the characteristic wing–like oscillations produced by the systems are generated only around the equilibria with a corresponding stability index I, while the equilibria of index II works as a commutation directing the orbit to either side. This wing-like oscillation, is possible only if the eigenvectors

of the equilibria are connected in such way that the trajectory oscillating exits from one unstable eigendirection to another stable one.

In the last decades, a tendency to design more complex dynamics in systems without considering the combination of the two types of equilibria with different stability indexes have emerged, *i.e.*, designing systems that produce oscillations around its equilibria considering only one of the two types of stability indexes I or II. The case of the stability index I is very common, the idea is to generate scrolls located along one or several axis [6, 7, 8, 12, 13, 14] forming grids. Each of the overall systems reported therein results in a switching heteroclinic orbit that changes domain oscillating chaotically between the equilibria. ~~On the other hand, the design of systems with only equilibria of stability index II is not as straightforward.~~ The complexity of designing circuits with stability index II lies on the intrinsic characteristic of the stable focus-saddle type equilibria and the narrow basin of attraction in which the orbit lies, since if the system is initialized outside the basin, the trajectory will increase without limits. Recently, an outstanding approach on generating homoclinic chaotic orbits from this type of stability index has come to light [9]. The idea of the method is to bound the trajectory of a system between at least two equilibria with stability index II.

The dynamics of this type of systems ~~usually~~ are studied and verified by numerical ~~integration methods~~ which are limited by discretization and computer memory ~~limitations~~. An effective alternative to solve this kind of complex problems can be found in analog, continuous-time computation [15, 16, 17]. One of the ideas proposed is to prove the feasibility of these methods by means of an electronic implementation [18, 19, 20]. ~~This physical~~ realization ~~made~~ by operational amplifiers and linear and nonlinear electronic components~~,~~ avoids ~~all~~ the numerical approximations ~~made by~~ the computer, resulting in a complete analog representation of the mathematical system. Usually, the electronic implementation of the systems with stability index I are easier to implement, because of the large basins of attraction in which the system lives. This is not the case for the systems of stability index of type II. Due to the high instability of the system and wether or not the initial conditions fall into the basins of

attraction, the electronic implementation of systems with only equilibria of the stability index type II results in a difficult and interesting challenge.

In order to attend this matter, the electronic implementation of two hybrid dynamical systems designed with a switching circuit based only on equilibria of stability index II that produces a homoclinic chaotic orbit is presented. The resulting orbit is trapped between the commutation surface which divides the two domains corresponding to the two equilibria of the system. The article is organized as follows: Section 2 presents the general theory that envelops the generation of UDS; Section 3 introduces the physical implementation of a UDS of type II; Section 4 discusses the experimental observations and finally conclusions are drawn in Section 5.

2. UDS theory

Consider the class of hybrid linear system given by

$$\dot{\mathbf{X}} = \mathbf{A}\mathbf{X} + \mathbf{B}, \tag{1}$$

where $\mathbf{X} = [x_1, x_2, x_3]^T \in \mathbf{R}^3$ is the state vector, $\mathbf{B} = [B_a, B_b, B_c]^T \in \mathbf{R}^3$ stands for a discrete real afine vector, $\mathbf{A} = [a_{ij}] \in \mathbf{R}^{3\times 3}$ with $i, j = 1, 2, 3$ denotes a linear matrix. This type of system presents its equilibrium point located at $X^* = -\mathbf{A}^{-1}\mathbf{B}$. Following the same notation as in [9], a system with stability index of the type II will be addressed as a system of the UDS type II. Therefore, two considerations have to be made in order to call Eq. (1) an UDS of type II and that it generates an attractor $\mathfrak{A}$.

a) The system must satisfy the dissipative condition $\sum_{i=1}^{3} \lambda_i < 0$, where $\lambda_i, i = 1, 2, 3$, are eigenvalues of $\mathbf{A}$. Consider also that one λ_i is a positive real eigenvalue, and two λ_i are complex conjugate eigenvalues with negative real part $Re\{\lambda_i\} < 0$, resulting in a stable focus-saddle equilibrium X^*. This type of equilibria presents an unstable manifold M^u with a fast eigendirection and a stable manifold M^s with a slow spiral eigendirection.

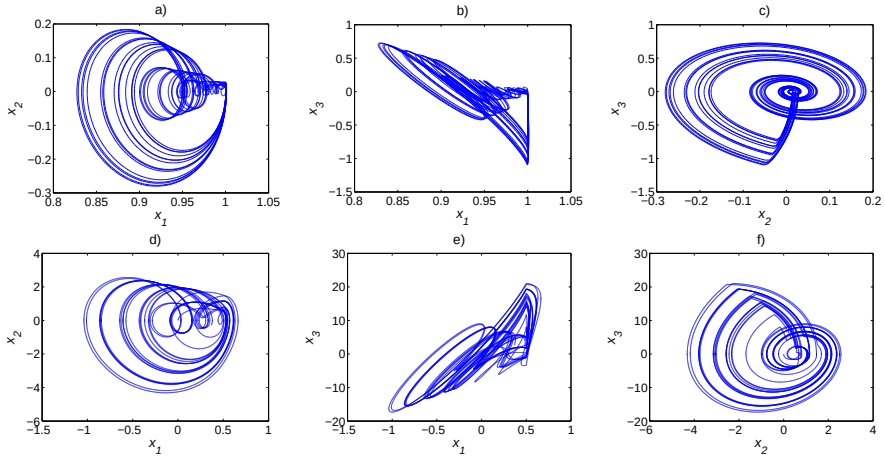

Figure 1: Projections of the attractor of the System A from eq. (3) with (4) onto the: a) (x_1, x_2) plane; b) (x_1, x_3) plane; c) (x_2, x_3) plane, with initial condition $X_0 = (1, 0, 0)$. Projections of the attractor of the System B from eq.(6) with (7) onto the: d) (x_1, x_2) plane; e) (x_1, x_3) plane; f) (x_2, x_3) plane, with initial condition $X_0 = (0, 0, 0)$. Results obtained from the numerical simulation of the systems.

b) The afine vector $\mathbf{B}$ must be considered as a discrete function that changes depending on which domain $\mathcal{D}_i \subset \mathbf{R}^3$ the orbit is located. Accordingly $\mathbf{R}^3 = \cup_{i=1}^{k} \mathcal{D}_i$. Then a hybrid system based on the continuous linear system (1) and the discrete function $\mathbf{B}$ is given by:

$$\dot{\mathbf{X}} = \mathbf{A}\mathbf{X} + \mathbf{B}(\mathbf{X}),$$

$$\mathbf{B}(\mathbf{X}) = \begin{cases} B_1, & \text{if } X \in \mathcal{D}_1; \\ B_2, & \text{if } X \in \mathcal{D}_2; \\ \vdots & \vdots \\ B_k, & \text{if } X \in \mathcal{D}_k. \end{cases} \tag{2}$$

The equilibria of system (2) are $X_i^* = -\mathbf{A}^{-1}B_i$, with $i = 1, \ldots, k$, and each entry B_i of the hybrid system will be considered in order to preserve the stability of system (2). To exemplify the theory of UDS of type II, two different systems will be considered.

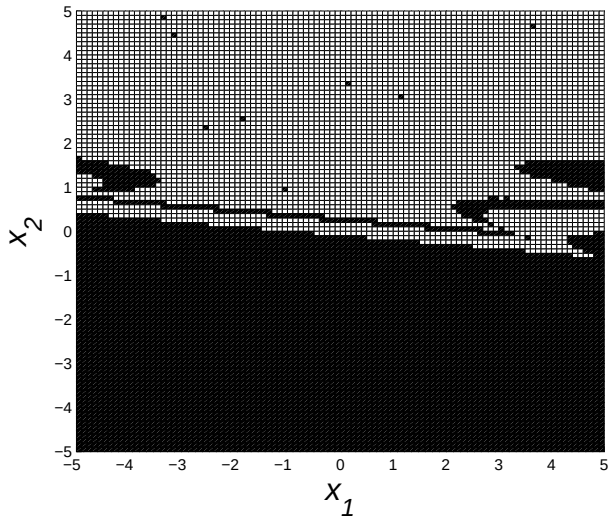

Figure 2: Projection of the basin of attraction of the system (2) with (3) onto the (x_1, x_2) plane with $x_3 = 0$. Marked with white the initial conditions that fall into the attractor.

2.1. System A

The first one is given in the same form as in [9] as follows:

$$\mathbf{A} = \begin{pmatrix} 0 & 1 & 0 \\ 0 & 0 & 1 \\ 0.15 & -10 & -1 \end{pmatrix}, \mathbf{B} = \begin{pmatrix} 0 \\ 0 \\ B_c \end{pmatrix}, \tag{3}$$

where B_c commutes according to the value of x_1 as follows:

$$B_c(x_1) = \begin{cases} -10, & \text{if } x_1 \geq 1; \\ 0 & \text{otherwise.} \end{cases} \tag{4}$$

The commutation surface is located at the $x_1 = 1$ plane. With this commutation law, the hybrid system results with the corresponding equilibrium points $X_1^* = (0, 0, 0)$ and $X_2^* = (66.6667, 0, 0)$, displacing only along the x_1 axis. In case that a displacement along different axes is intended, a different commutation law and surface should be designed.

It is also important to mention that due to the unstable properties of the focus-saddle equilibria, this dynamical system presents only one narrow region of

stability and an attractor is intended to be formed between the equilibrium point of the system. Meaning that at least two equilibrium points previously located are needed to trap the trajectory between them. The basin of attraction of the system was calculated by means of a numerical simulation in order to visualize this. Figure 2 depicts the projection of the basin onto the plane (x_1, x_2) with $x_3 = 0$, considering some of the possible values that the circuit may present at the moment of being energized. The white boxes present initial conditions that fall in the attractor, while the black boxes are initial conditions that escape to infinity. It can be appreciated that for values of $x_2, x_3 = 0$ when $x_1 < 0$ none of the initial conditions fall into the attractor. Notice that even for $(0, 0, 0)$ the trajectory escapes the attractor. Therefore the initial condition in which the system is initialized must be considered between the equilibria, preferably along the x_1 axis, otherwise the system will be initialized out of the basin of attraction and then expand to infinity. This is one of the main difficulties on working with systems that fall in the UDS type II category. Figure 1 a), b), and c) depicts the projections of the attractor generated by the system (3) with (4) onto the (x_1, x_2), (x_1, x_3) and (x_2, x_3) planes, respectively. In Figure 1 a) and b) it can be appreciated the trapped homoclinic attractor between the commutation surface oscillating between the equilibria. Notice that the size of the attractor is very small, oscillating only between $0.8 \geq x_1 \geq 1.05$.

By a further analysis of the system some basic properties are described next. The eigenvalues of (3) are $(0.0150, -0.5075 \pm 3.1237i)$, corresponding to the unstable focus equilibrium point mentioned above. The largest Lyapunov exponent of the system was calculated by the approach described by Wolf *et. al.* [21], resulting in the positive value 0.015, proving it is chaotic.

The volume density $\mathbf{V}(t)$ of the system given by Eq. (3) may be determined by the divergence of the flow, represented as follows:

$$\nabla \mathbf{V} = \frac{\partial \dot{x_1}}{\partial x_1} + \frac{\partial \dot{x_2}}{\partial x_2} + \frac{\partial \dot{x_3}}{\partial x_3} = -1, \tag{5}$$

hence the system is dissipative. Another important property is that the system

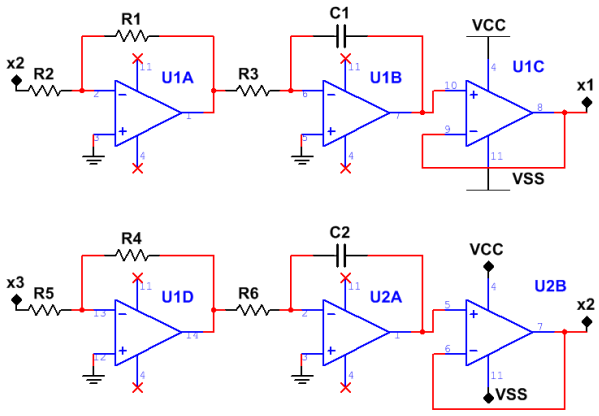

Figure 3: Schematic diagram of the x_1 and x_2 states of System A from eq. (2) with (3) and (4).

$\dot{\mathbf{X}} = \mathbf{AX}$ presents a natural symmetry under the transformation $(x_1, x_2, x_3) \mapsto (-x_1, -x_2 - x_3)$, therefore, a new hybrid system may be designed in order to generate a symmetric attractor.

2.2. System B

The second system to be analyzed will be given by:

$$\mathbf{A} = \begin{pmatrix} 0 & 0.1 & 0 \\ 0 & 0 & -0.1 \\ -1.3 & 2.5 & -0.15 \end{pmatrix}, \mathbf{B} = \begin{pmatrix} 0 \\ 0 \\ B_c \end{pmatrix}, \tag{6}$$

where B_c also commutes according to the value of x_1 as follows:

$$B_c(x_1) = \begin{cases} 10, & \text{if } x_1 \geq 0.5; \\ -1 & \text{otherwise.} \end{cases} \tag{7}$$

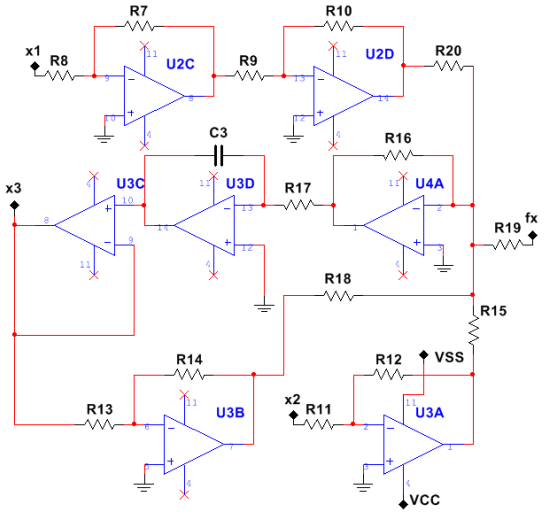

Figure 4: Schematic diagram of the x_3 state of the System A form eq. (2) with (3) and (4).

In this case the commutation surface is located at the $x_1 = 0.5$ plane. The hybrid system results with two equilibrium points $X_1^* = (7.6923, 0, 0)$ and $X_2^* = (-0.7692, 0, 0)$ from the commutation law. The corresponding eigenvalues result in $(0.05, -1 \pm 0.5i)$, assuring that the system falls into the scope of the UDS type II systems. The divergence of the system in the same way as the eq. (5) results in $\nabla \mathbf{V} = -0.15$. The largest Lyapunov exponent of the system results in the positive value 0.6027. Due to the dynamics of the system, the attractor is also trapped in the commutation surface oscillating between the equilibria. This can be appreciated from the projections of the attractor onto the (x_1, x_2), (x_1, x_3) and (x_2, x_3) planes depicted in Figure 1 d), e) and f), respectively. Similar considerations as in System A regarding the initial conditions must be taken in order to trap the trajectory of the system. In this case, the attractor presents a much greater oscillation bounded between $-1.5 \geq x_1 \geq 1$, but the position of the attractor also corresponds to the commutation surface at $x_1 \geq 0.5$. Notice

that even the form of the attractors is very similar due to the instability of the equilibria.

Now that both systems have been analyzed, the electronic implementation will be described next.

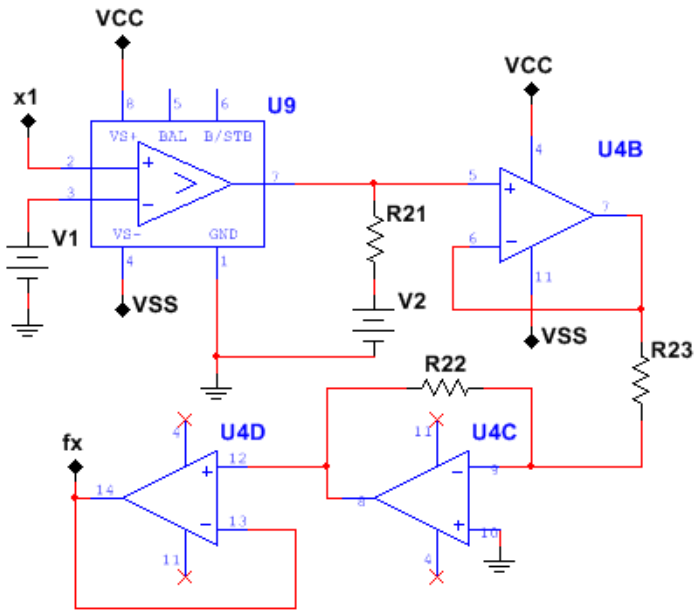

Figure 5: Schematic diagram of the hybrid System A from eq. (4) respect to the value of x_1.

3. Tri-Stable Electronic Circuit Implementation

The electronic implementation of both systems was realized considering the properties of analog computing through the operational amplifiers (Op-Amps) as described in [15]. The principal advantage of this type of components is that the output they provide is completely analog, meaning that the response of the circuit will be exactly what the equations describe. This represents a great advantage in comparison to microcontrollers or any other digital components which discretize the results. Besides, any change that need to be implemented in the value of parameters can be easily carried out by changing the linear value

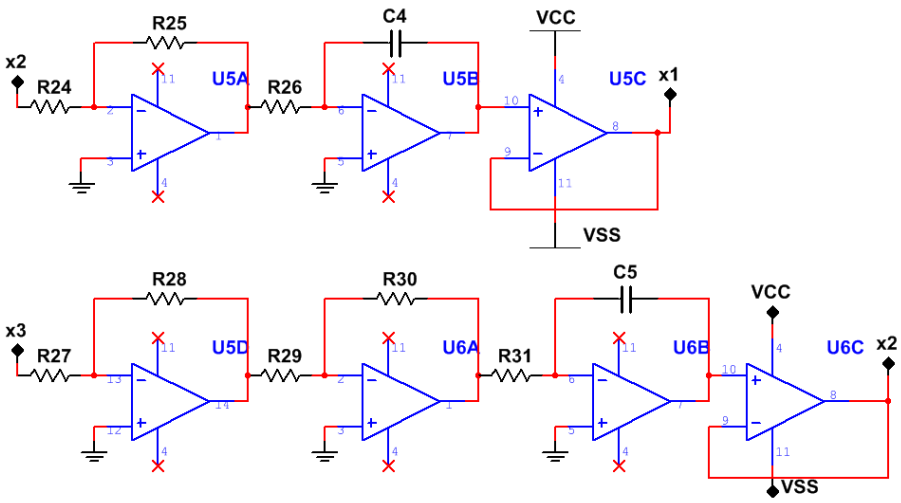

Figure 6: Schematic diagram of the x_1 and x_2 states of System B from eq. (2) with (6) and (7).

of the resistors, in comparison to circuits based on nonlinear components such as inductor and capacitors.

The configurations of the Op-Amp were implemented as follows, the equations of System A given by (2) with (3) are $\dot{x_1} = x_2$, $\dot{x_2} = x_3$ and $\dot{x_3} = 0.15x_1 - 10x_2 - x_3 + B_c(x_1)$. Integrating both sides of the equations will result in $x_1 = \int x_2 dt$, $x_2 = \int x_3 dt$ and $x_3 = \int (0.15x_1 - 10x_2 - x_3 + B_c(x_1))dt$, which can be implemented through an integration configuration. The summation on x_3 can be implemented with the summing configuration of the Op-Amp, and the parameter multiplication can be realized by adjusting the values of the resistors in the amplifying properties of the inverse amplifier configuration.

The schematic diagram of the electronic implementation of the System A is depicted in Figures 3 and 4. The first and second equations of System A from eqs. (2) with (3) were implemented by the Op-Amps U1A, U1B and U1C, and U1D, U2A and U2B of Figure 3, connected in inverting amplifier, inverting integrator and voltage follower configurations, respectively.

The third state is represented by U2C, U2D, U3A-U3D and U4A from Figure 4. Here the states x_1, x_2 and x_3 along with their corresponding coefficients are

obtained with U2C,U2D, U3A and U3B in inverting amplifier configuration, respectively. The signals generated are added along with the output of the commutation law fx (which corresponds to B_c) in U4A in a summing amplifier configuration and then integrated in U3A continued by a voltage follower to stabilize the output. The discrete function **B** given by Eq. (4) that changes between B_1 and B_2 depending on the values taken from the x_1 state, is developed by the circuit shown in Figure 5. This circuit was generated with U4B-U4D and U9, connected in an inverting amplifier and comparator configurations, comparing the state x1 with the constant voltage of V1 through a LM319N component.

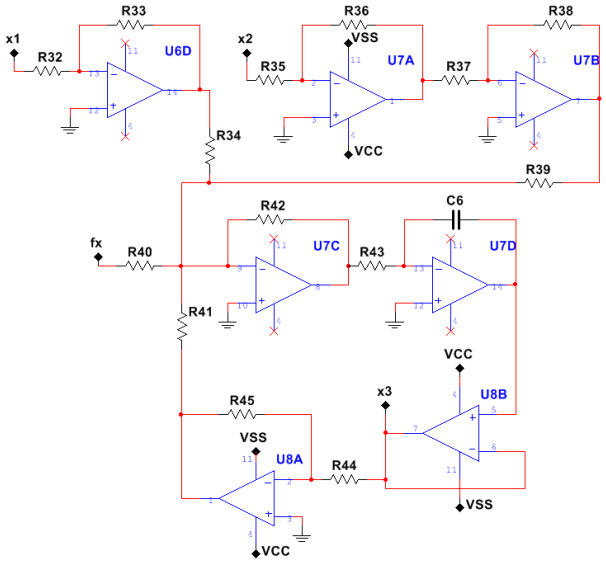

Figure 7: Schematic diagram of the x_3 state of System B from eq. (2) with (6) and (7).

By the analysis of the three output signals, $x1, x2$ and $x3$ given by the U1C, U2B and U3C Op-Amps, which correspond to x_1, x_2, x_3, respectively, the equations of the System A will result in the following equation:

$$
\begin{aligned}
x1 &= \tfrac{-1}{R3\cdot C1}\int\left(-\tfrac{R1}{R2}x2\right)dt - V_{C1_0},\\
x2 &= \tfrac{-1}{R6\cdot C2}\int\left(-\tfrac{R4}{R5}x3\right)dt - V_{C2_0},\\
x3 &= \tfrac{-1}{R17\cdot C3}\int\left(-\tfrac{R7\cdot R10\cdot R16}{R8\cdot R9\cdot R20}x1 + \tfrac{R12\cdot R16}{R11\cdot R15}x2 + \tfrac{R14\cdot R16}{R13\cdot R18}x3 - \tfrac{R16}{R19}fx\right)dt - V_{C3_0};
\end{aligned}
\tag{8}
$$

where R1-R19 identify the corresponding resistor value, C1-C3 the capacitor values, V_{C1_0}, V_{C2_0} and V_{C3_0} correspond to the initial voltage on the capacitors C1, C2, C3 respectively. Therefore, the initial conditions on the system must be considered throughout these capacitors. The oscillating frequency of the circuit is given by the integrator components in $R3 \cdot C1 = R6 \cdot C2 = R17 \cdot C3 = 1KHz$. Although internally the comparator works as an analog Op-Amp, the switching response is typically $80ns$. So this process can be considered as a discrete one, resulting in a digital and analog component system. Finally, the term fx, corresponds to the commutation law described in (4). All the values are displayed in Table 1.

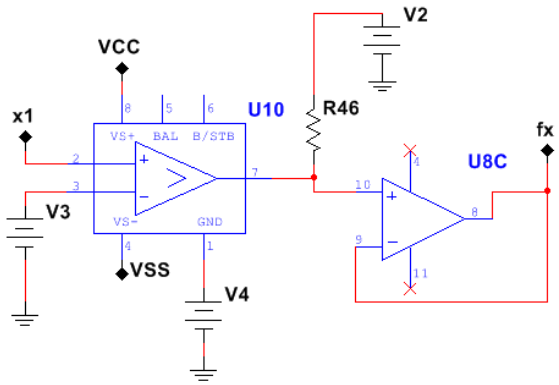

Figure 8: Schematic diagram of the hybrid System B from eq. (7) respect to the value of x_1.

In a similar way, the electronic implementation of the System B given by eq. (6) with (7), is depicted in the schematics from Figure 6 and 7. The x_1 and x_2 states are represented as the outputs $x1$ and $x2$ from the Op-Amps U5A-U5C

Table 1: Values and components of the electronic implementation. Any resistance not included here is consider with a value of 10kΩ.

Component	Value or name	Component	Value or name
R3,R6,R17,R26,R31,R43	1kΩ	U1-U4 & U5-U8	TL084IN
R7	1.5kΩ	U9 & U10	LM319N
R45	3kΩ	VCC	18V
R35,R44	20kΩ	VSS	-18V
R32	36kΩ	V1	1V
R33	47kΩ	V2	10V
R36	50kΩ	V3	0.5V
R12,R24,R27	100kΩ	V4	-1V
C1-C6	1μF		

and U5D, U6A-U6D in Figure 6, which are connected also as inverting amplifier and inverting integrator. The state x_3 is represented by the output signal $x3$ from Figure 6, which is obtained through the summing amplifier configuration of the Op-Amp U7C, and integrated in U7D. By the analysis of the three output signals, $x1, x2$ and $x3$ given by the U5C, U6C and U8B Op-Amps, which correspond to x_1, x_2, x_3, respectively, the equations of the System B will result in the following:

$$\begin{aligned} x1 &= \tfrac{-1}{R26\cdot C4}\int\left(-\tfrac{R25}{R24}x2\right)dt - V_{C4_0}, \\ x2 &= \tfrac{-1}{R31\cdot C5}\int\left(\tfrac{R28\cdot R30}{R27\cdot R29}x3\right)dt - V_{C5_0}, \\ x3 &= \tfrac{-1}{R43\cdot C6}\int\left(\tfrac{R33\cdot R42}{R32\cdot R34}x1 - \tfrac{R36\cdot R38\cdot R42}{R35\cdot R37\cdot R39}x2 + \tfrac{R45\cdot R42}{R41\cdot R44}x3 - \tfrac{R42}{R40}fx\right)dt - V_{C6_0}; \end{aligned} \tag{9}$$

where R25-R43 identify the corresponding resistor value, C4-C6 the capacitor values with corresponding initial conditions V_{C4_0}, V_{C5_0} and V_{C6_0}, respectively. Finally, the term fx correspond to the commutation law described in (7), which is implemented by the Op-Amp U8C and the comparator U10 in Figure 8,

commuting between the voltage references V2 and V4 after comparing the state of $x1$ with the reference value of V3. All the values are also displayed in Table 1.

4. Experimental observation of the circuits

In order to measure the response of the systems it is important to consider the initial voltage on the capacitors, which act as the condition from where the circuits will be initialized. The oscillating activity of both circuits A and B is extremely sensitive to this initial voltage, since it may take the trajectory of the system out of its basin of attraction tending to increase the response without limit onto the Op-Amps saturation states. This is a difficult task to accomplish in the sense that at the moment of energizing the circuit after a long period of disconnection, the capacitors will be fully discharged (i.e. $V_{Ci}(t_0) = 0$ with $i = 1, \ldots, 6$). This results in some difficulties to System A which as said before, will not fall into the attractor for the initial value $(0, 0, 0)$ due to the noise presented in all implementation. However after a brief period of time the capacitors will begin to charge gradually, affecting in this procedure the initial state of the system. In numerical simulation this behavior is not presented because the initial condition can be given in the basin of attraction and there is not noise.

In order to solve this problem there are some possible consideration to be made, for example, charging the capacitors previously. Take for instance the circuit of System A. If an electric impulse is given to some of the capacitors before energizing the circuit, this will affect the initial state. The basin of attraction of Figure 2 may present a valid range of values to be implemented, but consider that this basin doesnt belong to the circuit itself. Small variations on the resistor values and analog components may result in a different basin, as mentioned Siegelmann and Fishman in [16].

By doing this precharge of the capacitors, the output of the states of both systems were measured in the oscilloscope, resulting in the voltage outputs

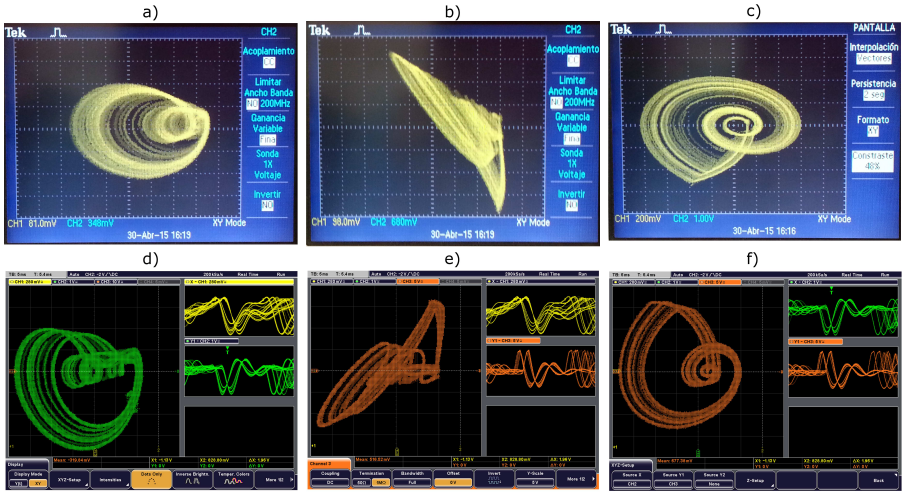

Figure 9: Voltage measures of the output signals of the System A in the oscilloscope: a) $x1$ vs $x2$, b) $x1$ vs $x3$, c) $x2$ vs $x3$. Output signals of System B: d) $x1$ vs $x2$, e) $x1$ vs $x3$, f) $x2$ vs $x3$.

screenshots given in Figure 9 for each corresponding system. It can be appreciated the similitude of the states calculated by means of numerical simulation in Figure 1 with the measured voltage of the electronically implemented circuit in Figure 9.

The second possibility regarding the instability due to the initial conditions, is to design an initial switching law in which the origin is taken between the equilibria and the trajectory of the attractor oscillates in the basin of attraction of the desired system. After this change to the desired switching law. The idea is as follows, two commutation laws are implemented. The first one $B_{n1}(x_m1)$ with $n1 = a, b, c$ and $m1 = 1, 2, 3$ considered from the time t_0 in which the circuit is energized, until a brief period of time t_i where the response of the circuit has been taken to a valid range of initial conditions. After t_i until t_∞, the switching law will be $B_{n2}(x_m2)$ with $n2 = a, b, c$ and $m2 = 1, 2, 3$.

To exemplify this, take the example of the System A. Instead of the commutation of (4) which results in the equilibria $X_1^* = (0, 0, 0)$ and $X_2^* = (66.6667, 0, 0)$. Consider the following commutation law:

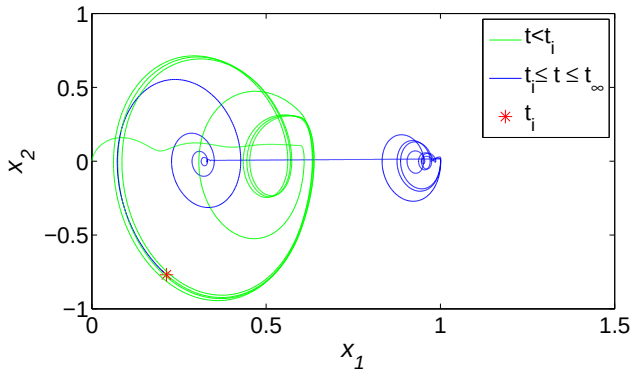

Figure 10: Projection of the attractor of the System A from eq. (3) with (10) for $t < t_i$ onto the (x_1, x_2) plane with initial condition $X_0 = (0, 0, 0)$. Marked with red line the trajectory for $t < t_i$. For $t_i \leq t \leq t_\infty$ the trajectory is marked with a blue line and the instant t_i is depicted with a green asterisk.

$$\begin{aligned} &\text{for } t < t_i \\ &\qquad B_{c1}(x_1) = \begin{cases} -10 & \text{if } x_1 \geq 0.6; \\ 1 & \text{otherwise;} \end{cases} \\ &\text{for } t_i \leq t \leq t_\infty \\ &\qquad B_{c2}(x_1) = \begin{cases} -10 & \text{if } x_1 \geq 1; \\ 0 & \text{otherwise.} \end{cases} \end{aligned} \tag{10}$$

With the commutation law from (10), System A will present the following equilibria: for $t < t_i$ $X_1^* = (-6.6667, 0, 0)$ and $X_2^* = (66.6667, 0, 0)$; for $t_i \leq t \leq t_\infty$ $X_1^* = (0, 0, 0)$ and $X_2^* = (66.6667, 0, 0)$. Now the initial condition $(0, 0, 0)$ falls between the equilibria as expected, and the trajectory of the system for $t < t_i$ oscillates in the positive range of x_1. This is depicted in the attractor of the system (3) with (10) in the numerical simulation projected for $t < t_i$ in Figure 10. In which for $t < t_i$ the trajectory is marked with a red line, the instant t_i is depicted with a green asterisk, and for $t_i \leq t \leq t_\infty$ the trajectory is marked with a blue line. The initial condition is $X_0 = (0, 0, 0)$. So the proposed method solves the problem of the saturation on the amplifiers previously discussed.

5. Concluding remarks

The electronic implementation based on two equilibrium points with stability index 2 using the UDS theory is presented. To generate a system whose trajectory oscillates between two of these points, it is necessary to design a hybrid system that changes to the closest equilibrium point of the subsystem whenever the trajectory is starting to move away from the actual equilibrium point. If the hybrid system is initialized far away of the commutation surface, the resulting systems will be unstable with no corresponding attractor. However, due to the saturation property of the op-amp the resulting circuit will not be unstable only fixed at saturated values. Since the system is built with components which present certain tolerance to their specific value, the circuit basin of attraction is fairly different to the proposed systems, causing in this saturation states instead of the oscillations at the moment of energizing it.

This type of circuits may be useful due to their easy-to-destabilized properties to some tilt detection applications, or in analog neuronal networks as described in [16, 17]. The study of this matter will be reported elsewhere.

6. Acknowledgements

L.J. Ontañón-García acknowledges the FAI-UASLP financial support through project No. C15-FAI-04-80.80. E. Campos-Cantón acknowledges CONACYT for the financial support through project No. 181002. The authors acknowledge the help given by M.C. Francisco Javier Cárdenas Flores in the circuit implementations and measurements.

References

[1] R. Goebel, R.G. Sanfelice, and A. Teel, Hybrid dynamical systems, Control Systems, IEEE, **29**(2), 28–93,(2009).

[2] W.M. Haddad, V. Chellaboina, S.G. Nersesov, Impulsive and hybrid dynamical systems, IEEE control systems magazine, (2006).

[3] K. Aihara and H. Suzuki, Theory of hybrid dynamical systems and its applications to biological and medical systems. Philosophical Transactions of the Royal Society A: Mathematical, Physical and Engineering Sciences, **368**(1930), 4893–4914, (2010).

[4] Taiji Suzuki, Nicholas Bruchovsky, Kazuyuki Aihara, Piecewise affine systems modelling for optimizing hormone therapy of prostate cancer, Philosophical Transactions of the Royal Society A: Mathematical, Physical and Engineering Sciences, **368**(1930), 5045-5059, (2010).

[5] E. M. Izhikevich, Hybrid spiking models, Philosophical Transactions of the Royal Society A: Mathematical, Physical and Engineering Sciences, **368**(1930), 5061–5070, (2010).

[6] E. Campos–Cantón, J. G. Barajas-Ramrez, G. Solis-Perales and R. Femat, (2010). Multiscroll attractors by switching systems. Chaos: An Interdisciplinary Journal of Nonlinear Science, **20**(1), 013116.

[7] E. Campos-Cantón, I. Campos-Cantón, J.S. González–Salas and F. Cruz–Ordaz, A parameterized family of single-double-triple-scroll chaotic oscillations, Rev. Mex. Fis. **54**(6), (2008).

[8] L. J. Ontañón–García, E. Jiménez-López, E. Campos–Cantón, M. Basin, A family of hyperchaotic multi-scroll attractors in $\mathbf{R}^n$, Appl. Math. Comput., **233**(2014).

[9] E. Campos-Cantón , R. Femat & Guanrong Chen. Attractors generated from switching unstable dissipative systems, CHAOS **22**, 033121, (2012)

[10] E. N. Lorenz, Synchronization of chaos, J. Atmos. Sci. **20**, 130, (1963).

[11] T. Matsumoto, A chaotic attractor from the Chua's circuit, IEEE Trans. Circuits Syst. I, 31(**12**), (1984).

[12] J. A. K. Suykens and J. Vandewalle. Generation of n-double scrolls ($n = 1; 2; 3; 4; ...$). IEEE Trans. Circuits Syst. I; **40**(11), pp. 861–867, (1993).

[13] M.E. Yalçin, J.A.K. Suykens, J. Vandewalle and S. Ozoguz, Families of scroll grid attractors, Int. J. Bifur. Chaos **12**(1), pp. 23–41, (2002).

[14] S. Yu, Y. Lü, Guanrong Chen and X. Yu, Generating grid multiwing chaotic attractors by constructing heteroclinic loops into switching systems, IEEE Trans. Circuits Syst. II; **58**(5) pp. 314–318, (2011).

[15] P. Orponen, A survey of continuous-time computation theory, In Advances in algorithms, languages, and complexity (pp. 209–224). Springer US, (1997).

[16] H.T. Siegelmann and S. Fishman, Analog computation with dynamical systems. Physica D: Nonlinear Phenomena, **120**(1), 214–235, (1998).

[17] Y. Horio and K. Aihara, Analog computation through high-dimensional physical chaotic neuro-dynamics, Physica D: Nonlinear Phenomena, **237**(9), 1215–1225, (2008).

[18] K. M. Cuomo and A. V. Oppenheim, Circuit implementation of synchronized chaos with applications to communications, Phys. Rev. Lett. **71**(1), (1993).

[19] G. Qia and Guanrong Chen, Analysis and circuit implementation of a new 4D chaotic system, Phys. Lett. A **352**, pp. 386-397, (2006).

[20] T. Gao, Guanrong Chen, Z. Chen and S. Cang, The generation and circuit implementation of a new hyper-chaos based upon Lorenz system, Phys. Lett. A **361**, pp. 78-86, (2007).

[21] A. Wolf, J.B. Swift, H.L. Swinney and J. Vastano, Determining Lyapunov exponents from a time series, Elsevier Science Publishers, Physica D, Vol. vol. **16**, pp. 285–317, (1985).